Proceedings of the ASME 2015 Pressure Vessels and Piping Conference
PVP2015
July 19-23, 2015, Boston, Massachusetts, USA

PVP2015-45672

FURTHER INSIGHTS ON THE RELATIONSHIP BETWEEN J AND CTOD FOR SE(B) AND SE(T) SPECIMENS INCLUDING DUCTILE CRACK PROPAGATION

Diego F. B. Sarzosa
Department of Naval Architecture
and Ocean Engineering
University of São Paulo, São Paulo, Brazil
Email:dsarzosa@gmail.com

Claudio Ruggieri
Department of Naval Architecture
and Ocean Engineering
University of São Paulo, São Paulo, Brazil
Email:claudio.ruggieri@usp.br

ABSTRACT

In structural assessment procedures the crack driving force is usually estimated numerically based on the J -Integral definition because its determination is well established in many finite element codes. The nuclear industry has extensive fracture toughness data expressed in terms of J-Integral and huge experience with its applications and limitations. On the other hand, material fracture toughness is typically measured by Crack Tip Opening Displacement (CTOD) parameter using the hinge plastic model or double clip gauge technique. The parameter CTOD has a wide acceptance in the Oil and Gas Industry (OGI). Also, the OGI has a lot of past data expressed in terms of CTOD and the people involved are very familiar with this parameter. Furthermore, the CTOD parameter is based on the physical deformation of the crack faces and can be visualized and understood in an easy way. There is a unique relationship between J and CTOD beyond the validity limits of Linear Elastic Fracture Mechanics (LEFM) for stationary cracks. However, if ductile crack propagation occurs, the crack tip deformation profile and stress-strain fields ahead of the crack tip will change significantly when compared to the static case. Thus, the stable crack propagation may change the well established relationship between J and CTOD for stationary cracks compromising the construction of resistance curves J-Δa from CTOD-Δa data or vice versa. This investigation is a complementary study on the relationship between J-Integral and CTOD under ductile crack propagation of a previous work. The theoretical definition of CTOD using the 90^o method and the empirical expression used in the standard ASTM E1820 are analyzed under stable crack growth. Plane-strain finite element computations including stationary and growth analysis are conducted for 3P SE(B) and clamped SE(T) specimens having different notch length to specimen width ratios in the range of 0.1-0.5. For the growth analysis, the models are loaded to levels of J consistent to a crack growth resistance curve representative of a typical pipeline steel. A computational cell methodology to model Mode I crack extension in ductile materials is utilized to describe the evolution of J with a. Laboratory testing of an API 5L X70 steel at room temperature using standard, deeply cracked C(T) specimens is used to measure the crack growth resistance curve for the material and to calibrate the key cell parameter defined by the initial void fraction, f_0 . The presented results provide additional understanding of the effects of ductile crack growth on the relationship between J-Integral and CTOD for standard and non-standard fracture specimens. Specific procedures for evaluation of CTOD-R curves using SE(T) and SE(B) specimens with direct application to structural integrity assessment and defect analysis in pipelines and risers will be proposed, yielding accurate and robust relations between J-Integral and CTOD.

INTRODUCTION

The Oil and Gas Industry has some bias to use CTOD as parameter to describe fracture toughness data [1]. On the other hand, crack driving forces can be easily characterized by J -Integral using finite element analysis. Both parameters have advantages and disadvantages. First, the J-Integral parameter has a robust mathematical definition, its determination is well established in all major commercial finite element codes. However,

the J-Integral dominance breaks down when excessive plasticity (large strain) spreads over the remaining ligament.

Second, CTOD parameter is based on the physical deformation of the crack faces and can be visualized and understood in an easy way . Theoretically, it does not have mathematical limitations regarding to the level of plastic deformation ahead of the crack tip or elastic unloading associated with crack growth or stress-strain relationship. Also, since CTOD is a physical parameter, it is often regarded as a simple, qualitative measure of material toughness, similar to charpy test [2].

CTOD parameter has no unique definition, that is, there is no single crack face displacement that can be regarded as characteristic property of the material. Also, the hinge plastic model typically used to measure CTOD assumes that crack faces remain straight, allowing the use of similar triangles to calculate CTOD , is not valid for materials with high hardening, low levels of plastic displacements and shallow cracks [3].

Currently, the American standard ASTM E1820-08 [4] defines the relationship between J-Integral and $CTOD$ via an empirical plastic constraint factor (m). This m factor is expressed as function of the crack size (a/W) and a measure of the strain hardening capacity defined by the ratio $\frac{\sigma_{YS}}{\sigma_{TS}}$, where σ_{YS} is the yield strength and σ_{TS} is the ultimate tensile strength.

Recently, the American Society for Testing and Materials (ASTM) substantially modified its methodology for assessing the parameter $CTOD$ in its procedures ASTM E1290-08 [5] (and, consequently, also the ASTM E1820-08 [4]) using specimens SE(B), and C(T). The current approach is now based on the determination of the J- Integral (usually through the plastic work approach using load versus displacement measurements - CMOD or LLD) followed by its conversion to a corresponding value of CTOD. Therefore, as a material fracture toughness property, the J parameter is measured using the area under the load-displacement curve (U), so J is directly proportional to U. In contrast, according to the hinge plastic model, δ is proportional to plastic component of the mouth opening displacement. Thus, the relationship between both parametesr depend on strain hardening and the level of crack tip constraint [2].

Shih [6] showed a unique relationship exists between J and $CTOD$ beyond the validity limits of Linear Elastic Fracture Mechanics (LEFM). Rice, by a private communication, suggested an operational definition of the crack-tip opening displacement as the opening distance between the intercept of two 45^o-lines, drawn back from the tip with the deformed profile as illustrated in Fig. 1:

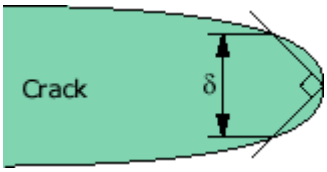

FIGURE 1. CMOD definition by displacement at the intersection of a 90° vertex with the crack flanks

Shih using the Hutchinson and Rice and Rosengren (HRR) singularity to estimate the crack-tip displacements obtained the following relation [6]:

$$\delta = d_n \frac{J}{\sigma_{YS}} \tag{1}$$

where δ is the crack-tip opening displacement, σ_{YS} is the yield stress, and d_n is a dimensionless constant.

Shih [6] stated that a unique relationship between J and δ , as defined by Eq. (1), requires that the HHR field dominates the crack-tip deformation over a size scale at least of the order of one CTOD . The annular sector size ($\bar{R}$) where the HHR singularity dominated decreases for low hardening materials and vanishes at the limit of non-hardening material. Therefore, a unique relationship between J and δ for non-hardening material may not exist. In contrast, for hardening materials in Small Scale Yielding (SSY) condition a unique relationship between J and δ has been proven to exist. Under Large Scale Yielding (LSY) condition for hardening materials subjected primarily to bending Eq. (1) is still valid, but for structures subjected primarily to tensile loading and have moderate and low hardening capacity Eq. (1) is not valid and produce δ estimations, based on J values, lower than finite element analysis based on small strain theory and J_2 flow theory of plasticity reported by Shih [6].

Engineering Critical Assessment (ECA) procedures applicable to reeled pipes [7] rely on direct applications of $J\,(CTOD)$-resistance data measured using small, laboratory fracture specimens to specify acceptable flaw sizes. These approaches allow the specification of critical crack sizes based on the predicted growth of crack-like defects under service conditions. Current standardization efforts now underway [8, 9, 10] advocate the use of single edge notch tension specimens (often termed SE(T) crack configurations) to measure experimental R-curves more applicable to high pressure piping systems and girth welds of marine steel risers. The primary motivation to use SE(T) specimens to describe the fracture toughness curve is the similarity in the crack tip fields (stresses and strains), which control the fracture process, between the non-standardized SE(T) geometry and pipeline girth welds under bending as SINTEF's work showed

[11].

The SE(T) geometry generally develops low levels of crack-tip stress triaxiality (associated with the predominant tensile loading which develops during the fracture test) thereby contrasting sharply to conditions present in deeply cracked SE(B) and C(T) specimens. Recent applications of SE(T) fracture specimens to characterize crack growth resistance properties in pipeline steels [12] have been effective in providing larger flaw tolerances while, at the same time, reducing the otherwise excessive conservatism which arises when measuring the material's fracture toughness based on high constraint, deeply-cracked, SE(B) specimens.

However, crack growth can change the specimen (real structure) constraint having big implications for ECA procedures. Under crack propagation the stress-strain fields ahead of the crack tip changes significantly, when compared to the static case, and thus constraint similarity between SE(T) and pipeline may be lost. Also, stable crack propagation may change the well established relationship, under Small Scale Yielding (SSY) conditions, between J and $CTOD$, see Eq. (1), for stationary cracks, compromising the construction of resistance curves $CTOD - \triangle a$ from $J - \triangle a$ curves. Therefore, during fracture assessments of critical structures, including piping and marine facilities, is necessary to know accurate relationships between the J -Integral and CTOD parameters.

Although conceptually simple and directly connected with fundamental methodologies for determining the J Integral (such as η methodology [9, 13, 14]), there are no J vs. δ relations specifically developed for SEN(T) specimens or reeled pipelines. Perhaps more importantly, few and limited relationships between J and $CTOD$ are available in the scientific and technical literature and do not explicitly consider the evolution of $CTOD$ when the crack is under stable propagation mode I. Indeed, as illustrated schematically in Fig. 2, the ductile crack extension changes the crack tip profile and it has a great impact on the correct definition of $CTOD$. Also, Fig. 2 shows additional definitions to measure $CTOD$ for growing cracks.

This research includes the study and development of more accurate and appropriate relationships between J and $CTOD\,(\delta)$. The main goal is to provide a comprehensive set of expressions between J and δ for SEN(T) and SE(B) geometries in order to allow the determination of resistance $CTOD - R$ curves from $J - R$ curves or vice versa. Also, two possible definitions of δ during crack growth are explored in order to check the best linear correlation with J; see Fig.2 for ilustration of these definitions. These analyses include stationary and crack growth plane-strain results to determine J and $CTOD$ for these cracked configurations. Laboratory testing of an API X70 steel at room temperature using standard deeply cracked C(T) specimens is used to measure the crack growth resistance curve for the material and to calibrate the key micro-structural parameter utilized in the growth analysis. The numerical computations show a rather marked difference between the $J - CTOD$ relationship for stationary and growth analysis with important implications for experimental measurements of $CTOD$-resistance curves. Therefore, this work provides a body of results which enables establishing accurate relationships between J and $CTOD$ for use in testing protocols for toughness measurements.

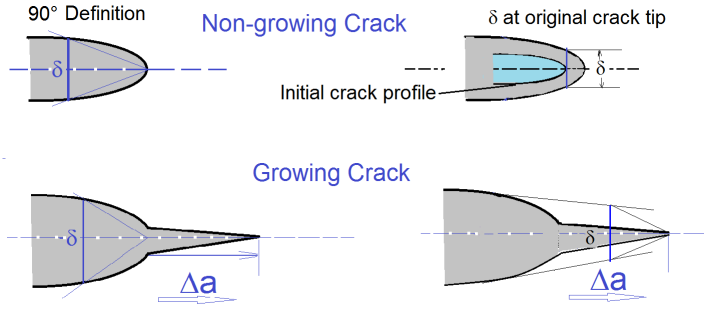

FIGURE 2. Ilustration of possible definitions of CTOD for growing cracks

J AND CTOD EVALUATION PROCEDURE

Estimation Procedure Based on Plastic Work

Evaluation of the J-integral from laboratory measurements of load-displacement records is most often accomplished by considering the elastic and plastic contributions to the strain energy for a cracked body under Mode I deformation [15] as follows

$$J = J_e + J_p \tag{2}$$

where the elastic component, J_e, is given by the standard form

$$J_e = \frac{K_I^2}{E'} \tag{3}$$

in which K_I is the (Mode I) elastic stress intensity factor and $E' = E$ or $E' = E/(1-\nu^2)$ whether plane stress or plane strain conditions are assumed with E representing the (longitudinal) elastic modulus. Here, solutions for the elastic stress intensity factor, K_I , for a SE(B) specimen are given by Tada et al. [16] whereas Cravero and Ruggieri [17] provide wide range K_I-solutions for pin-loaded and clamped SE(T) specimens.

The plastic component, J_p, is conveniently evaluated from the plastic area under the load-CMOD curve as

$$J_p = \frac{\eta_J A_p}{bB} \tag{4}$$

where A_p is the plastic area under the load-CMOD curve and factor η_J represents a nondimensional parameter which describes the effect of plastic strain energy on the applied J. The previous definition for J_p derives from the assumption of nonlinear elastic material response thereby providing a deformation plasticity quantity. Figure 3 schematically illustrates the procedure to determine the plastic area to calculate J from typical load-CMOD records in which the crack mouth opening displacement is often also denoted V.

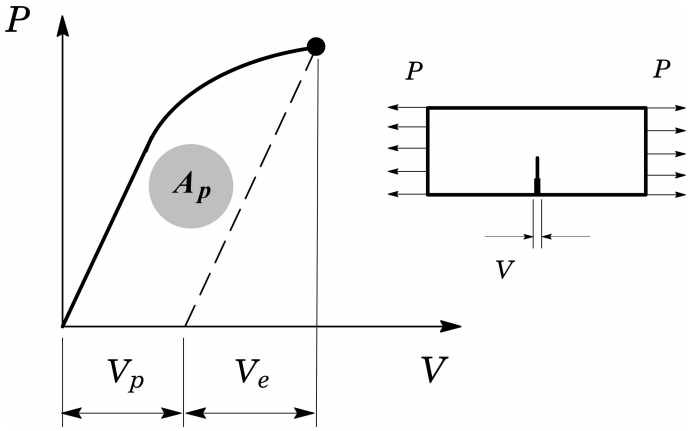

FIGURE 3. Plastic area under the load-displacement (CMOD) curve for a fracture specimen.

CTOD Evaluation Procedure

The previous framework also applies when the CTOD is adopted to characterize the crack-tip driving force. Following the earlier analysis for the J-integral and using the connection between J and the crack-tip opening displacement (δ), given by Eq. (1), yields the following relationship:

$$\delta = \delta_e + \delta_p \tag{5}$$

where the elastic component, δ_e, is given by

$$\delta_e = \frac{K_I^2}{m_{SSY}\sigma_{ys}E'} \tag{6}$$

and the plastic component, δ_p, is expressed as

$$\delta_p = \frac{\eta_\delta A_p}{bB\sigma_{ys}} \tag{7}$$

where factor η_δ now represents a nondimensional parameter which describes the effect of plastic strain energy on the applied CTOD. In the above expressions, m_{SSY} is a plastic constraint factor relating J and CTOD under small scale yielding [15], σ_{ys} denotes the material's yield stress and parameter m represents a proportionality coefficient often used to relate the total value of J to the total value of CTOD which strongly depends on the material's strain hardening [6, 18]. The η_δ factors were reported for SE(B) and clamped SE(T) geometries in previous work [19].

NUMERICAL PROCEDURES

Finite Element Models for Stationary Crack Analyses

Nonlinear finite element analyses are described for plane-strain models of bend and tension loaded crack configurations covering 1-T plane-sided SE(B) and SE(T) fracture specimens with fixed overall geometry having thickness B =25.4 mm and varying crack sizes. The analysis matrix includes standard SE(B) specimens ($S/W = 4$) and clamped SE(T) specimens ($H/W = 10$) with $W/B = 2$ having $a/W = 0.10$ to 0.7 with increments of 0.05. Here, a is the crack size, W is the specimen width, S defines the specimen span for the bend configuration and H represents the distance between clamps for the tension specimen. Figure 4 shows the geometry and specimen dimensions for the analyzed crack configurations.

Figure 5 shows the finite element models constructed for the plane-strain analyses of the clamped SE(T) specimen having $a/W = 0.5$ for stationary crack analysis. All other crack models have very similar features. A conventional mesh configuration having a focused ring of elements surrounding the crack front is used with a small key-hole at the crack tip; the radius of the key-hole, ρ_0, is 2.5 μm (0.0025 mm) to enhance computation of J-values at low deformation levels. Previous numerical analyses [17] reveal that such mesh design provides detailed resolution of the near-tip stress-strain fields which is needed for accurate numerical evaluation of J-values. Symmetry conditions permit modeling of only one-half of the specimen with appropriate constraints imposed on the remaining ligament. A typical half-symmetric model has one thickness layer of 1300 8-node, 3D elements ($\sim$2800 nodes) with plane-strain constraints ($w = 0$) imposed on each node. These finite element models are loaded by displacement increments imposed on the loading points to enhance numerical convergence.

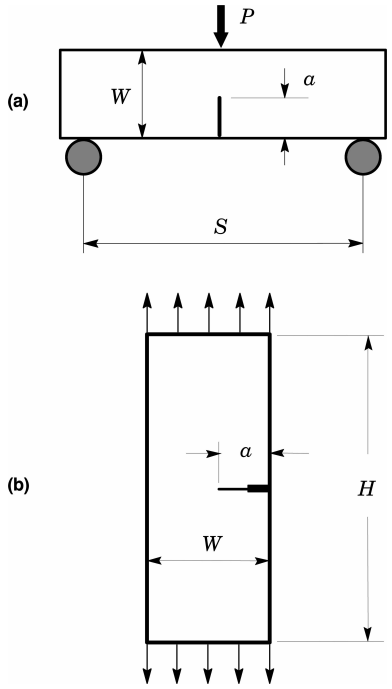

FIGURE 4. Specimen geometries and dimensions for analyzed crack configurations.

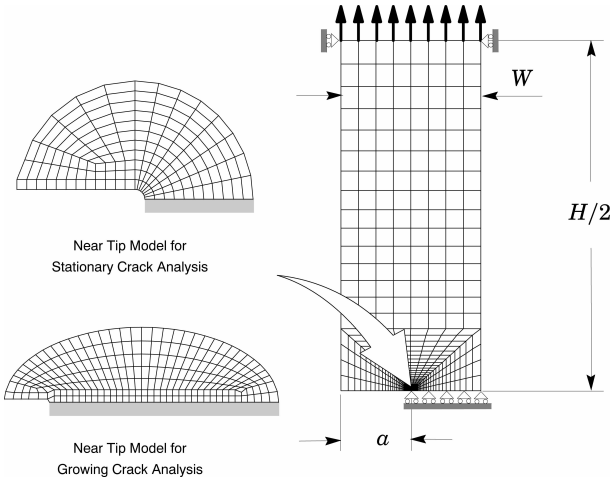

FIGURE 5. Plane-strain finite element model for the clamped SE(T) specimen with $a/W = 0.5$.

Numerical Models Including Ductile Tearing

Xia and Shih (X&S) [20] proposed an engineering approach based upon damage mechanics to predict *R*-curves for cracked configurations under ductile regime. Material separation occurs through a local fracture mechanism described by the micromechanics parameters D, which defines the thickness of the computational cell layer on which Mode I growth evolves and the initial cell porosity, f_0, which roughly represents the actual metallurgical features of the material. Progressive void growth and subsequent macroscopic material softening in each cell are described by a constitutive model for dilatant plasticity given by progressive void growth and subsequent macroscopic material softening in each cell are described with the Gurson-Tvergaard (GT) constitutive model for dilatant plasticity [21, 22] given by

$$\Phi(\sigma_e, \sigma_m, \sigma_0, f) = \frac{\sigma_e}{\sigma_0} - \omega(\sigma_m, \sigma_0, f) = 0 \tag{8}$$

$$\omega(\sigma_m, \sigma_0, f) = [1 - 2q_1 \cdot f \cdot cosh\left(\frac{3q_2 \cdot \sigma_m}{2\sigma_0}\right) - q_3 \cdot f^2]^{\frac{1}{2}} \tag{9}$$

where σ_e denotes the effective Mises (macroscopic) stress, σ_m is the mean (macroscopic) stress, σ_0 is the current flow stress of the cell matrix material and f defines the current void fraction. Here, factors q_1, q_2 and $q_3 = q_1^2$ are material constants. Using an experimental $J - \Delta a$ curve obtained from a conventional, deeply cracked SE(B) or C(T) specimen, a series of finite element analyses of the specimen are conducted to calibrate values for the cell parameters D and f_0 which bring the predicted $J - \Delta a$ curve into agreement with experiments as described later in the article. Readers are referred to the works of Xia and Shih [23], Ruggieri and Dodds (R&D) [24] and Gullerud et al. [25] for further details.

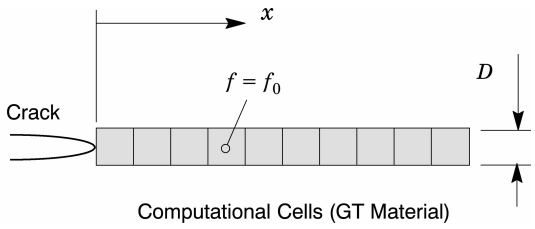

FIGURE 6. Computational cell model for ductile tearing.

To simulate ductile crack extension using the GT model, the planar meshes (2-D) for the SE(T) and SE(B) fracture specimens are similar to the plane-strain finite element models for stationary crack analyses described previously but contains a row of 60 computational cells along the remaining crack ligament $(W - a)$ as depicted in Fig. 6. Experience with past finite element analyses of fracture specimens to estimate the cell size for

common structural and pressure vessel steels suggests values of $50 \sim 200\,\mu$m for D [24, 25, 26]. Here, the cell size is adopted as $D/2 = 100\,\mu$m. This size provides an approximate correlation of spacing between the large inclusions and the crack tip opening displacement (CTOD) at the onset of macroscopic crack growth in conventional fracture specimens for common pressure vessel steels while, at the same time, providing adequate resolution of the stress-strain fields in the active layer and in the adjacent background material.

Calibration of the initial material porosity (void fraction), f_0, for the GT material requires a crack growth analysis to match R-curves obtained from testing of high constraint, deeply cracked specimens. Hippert [27] tested 1-T compact tension C(T) specimens ($B = 25.4$ mm) with $a/W = 0.65$ and 20% side-grooves (10% each side) to measure ductile tearing properties for the API X70 pipeline steel utilized in this study. The finite element mesh for the growth analysis of the deeply-cracked C(T) specimen contains a row of 120 computational cells along the remaining crack ligament $(W-a)$ with fixed size of $D/2 \times D/2$ (see Fig. 6). The initially blunted crack tip accommodates the intense plastic deformation and initiation of stable crack growth in the early part of ductile tearing. Symmetry conditions permit modeling of only one-half of the specimen with appropriate constraints imposed on the remaining ligament. This half-symmetric, plane-strain model has one thickness layer of 1611 8-node, 3D elements (3522 nodes) with plane-strain constraints ($w = 0$) imposed on each node and displacement increments imposed on the loading point which permits continuation of the analyses once the load decreases during crack growth.

Material Models and Finite Element Procedures

The elastic-plastic constitutive model employed in the stationary crack analyses reported here follows a flow theory with conventional Mises plasticity in small geometry change (SGC) setting. The numerical solutions for fracture specimens and cracked pipes utilize a simple power-hardening model to characterize the uniaxial true stress ($\bar{\sigma}$) *vs.* logarithmic strain ($\bar{\varepsilon}$) in the form

$$\frac{\bar{\varepsilon}}{\varepsilon_0} = \frac{\bar{\sigma}}{\sigma_0}\,,\ \varepsilon \le \varepsilon_0\ ;\ \ \frac{\bar{\varepsilon}}{\varepsilon_0} = \left(\frac{\bar{\sigma}}{\sigma_0}\right)^n\,,\ \varepsilon > \varepsilon_0 \qquad (10)$$

where σ_0 and ε_0 are the reference (yield) stress and strain, and n is the strain hardening exponent. The finite element analyses consider material flow properties covering typical structural, pressure vessel and pipeline grade steels with E =206 GPa and ν =0.3:$n = 5$ and E/σ_{ys} =800 (high hardening material), $n = 10$ and E/σ_{ys} =500 (moderate hardening material) and $n = 20$ and E/σ_{ys} =300 (low hardening material).

For the crack growth analyses, the mechanical and flow properties for the API 5L X70 pipeline grade steel tested by Hippert [27] are employed to generate the required numerical solutions in large geometry change (LGC) setting. The material has 484 MPa yield stress (σ_{ys}) and 590 MPa tensile strength (σ_{uts}) at room temperature (20°C) with relatively moderate-to-low hardening properties ($\sigma_{uts}/\sigma_{ys} \approx 1.22$). Additional material properties include Young's modulus E =205 GPa and Poisson's ratio ν =0.3. Based on Annex F of API 579 [28], the Ramberg-Osgood strain hardening exponents describing the stress-strain response for the tested API 5L X70 pipeline grade steel is estimated as $n = 13.3$ Further, to describe the evolution of void growth and associated macroscopic material softening in the computational cells, the GT constitutive model given by Eq. (8) is adopted. The background material outside of the computational cells follows a flow theory with the Mises plastic potential obtained by setting $f \equiv 0$ in Eq. (8). The uniaxial true stress-logarithmic strain response for both the background and cell matrix materials follows a piecewise linear approximation to the measured tensile response for the material at room temperature given in Hippert [27]. The two adjustment factors in the Gurson yield condition given by Eq. (8) are taken from the work of Faleskog and Shih [29] as $q_1 = 1.43$ and $q_2 = 0.97$.

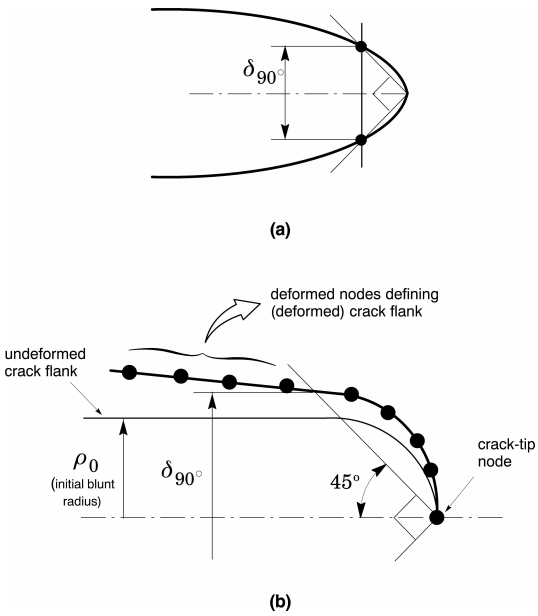

FIGURE 7. a) Definition of CTOD based on the 90° intercept procedure; b) Adopted numerical strategy to evaluate the CTOD.

The finite element code WARP3D [30] provides the numerical solutions for the plane-strain simulations reported here including stationary and crack growth analyses implementing the cell model. The research code FRACTUS2D [30] is employed to

compute the $J-$CTOD relationships derived from stationary and growth analyses for the analyzed fracture specimens. Evaluation of the numerical value of CTOD follows the 90° procedure [15] to the deformed crack flanks. To avoid potential problems with the CTOD computation related to the severe mesh deformation at the crack tip, the approach adopted here defines the value of half the crack tip opening displacement as the intercept between a straight line at 45° from the crack tip and a straight line passing through selected nodes at the crack flank as illustrated in Fig. 7. The straight line defined by the deformed crack flank nodes is obtained by a linear regression of the corresponding nodal displacements.

Calibration of Cell Parameters

Numerical simulation of ductile tearing in the fracture specimens described here begins with calibration of the cell parameters, f_0 and D, for the pipeline steel employed in this study. The cell size D and initial porosity f_0 define the key parameters coupling the physical and computational models for ductile tearing. The measured resistance curve for a deeply cracked C(T) specimen ($a/W = 0.65$) tested by Hippert [27] (see also Hippert and Ruggieri [31]) using the unloading compliance technique is employed to calibrate these parameters. Within the present context, a series of finite element analyses is conducted to calibrate the cell parameters which establish agreement between the predicted $J-\Delta a$ curve and experiments for a high constraint fracture specimen.

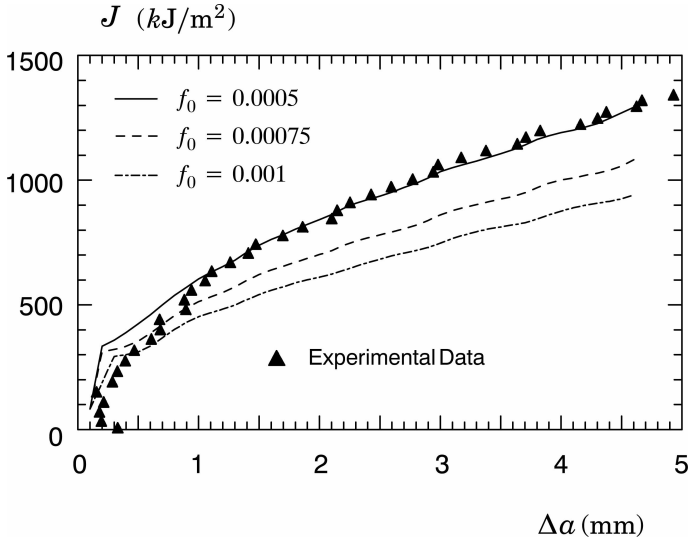

FIGURE 8. Comparison of measured and predicted R-curve with different f_0-values for side-grooved 1-T C(T) specimen of API 5L-X70 at room temperature.

Figure 8 displays the measured crack growth resistance curve (average of two tests) in the TL orientation (described by the solid symbols in the plot) for the tested pipeline steel at room temperature. This fracture data was obtained using conventional 1-T C(T) specimens having the following dimensions: gross thickness, $B = 25$ mm, net thickness, $B_n = 20$ mm (20% side groove), width, $W = 50$ mm, $a = 32.5$ mm ($a/W = 0.65$). Hippert and Ruggieri [31] provide additional details of the material properties, including metallurgical characterization, and the fracture tests.

As described earlier, we specify the cell size $D/2 = 100\,\mu$m for the API X70 material employed in this study. Hence, with parameter D fixed, the calibration process then focuses on determining a suitable value for the initial volume fraction, f_0, that produces the best fit to the measured crack growth data for the deeply cracked C(T) specimen. Figure 8(b) also shows the predicted $J-\Delta a$ curves for this specimen. Predicted R-curves are shown for three values of the initial volume fraction, f_0 =0.0005, 0.00075 and 0.001. For $f_0 = 0.0005$, the predicted R-curve agrees well with the measured values for almost the entire range of growth, albeit lying a little above the measured data for $\Delta a \leq 1$ mm in the blunting line region. In contrast, the use of $f_0 = 0.001$ produces a much lower resistance curve relative to the measured data. Consequently, the initial volume fraction $f_0 = 0.0005$ is thus taken as the calibrated value for the API 5L-X70 steel used subsequently in this study.

RESULTS

J-CTOD Relationship in Stationary Cracks

Figures 9-10 provide the variation of the J-integral with CTOD for the SE(B) and clamped SE(T) fracture specimens with different a/W-ratios and the moderate strain hardening material ($n = 10$). The trends and results described here are similar for other strain hardening materials; to conserve space, these results are not shown here.

Consider first the J-CTOD relationship for the SE(B) geometry displayed in Fig. 9(a). It can be seen that the J -CTOD relationship is relatively sensitive to a/W-ratio with increased levels of loading as measured by increased values of J. Figure 9(b) shows the evolution of parameter m with increased J for the analyzed SE(B) specimens. Here, the m-values display a strong variation at small levels of loading (as characterized by small J-values); such behavior derives directly from a strong nonlinear relationship between J and CTOD early in the loading of the specimen. After this transitional behavior, the m-values increase slowly with increased J and attain a constant value, albeit slightly dependent on the a/W-ratio, for larger levels of loading.

Consider next the J-CTOD relationship for the clamped SE(T) specimen displayed in Fig. 10.(a) In contrast to the previous results, observe that the J-CTOD relationship for the clamped SE(T) geometry is independent of the a/W-ratio. As a

consequence, after a transitional behavior at early stages of loading, parameter m for this crack configuration attains a constant value of ~ 1.65 for the entire range of a/W-ratio.

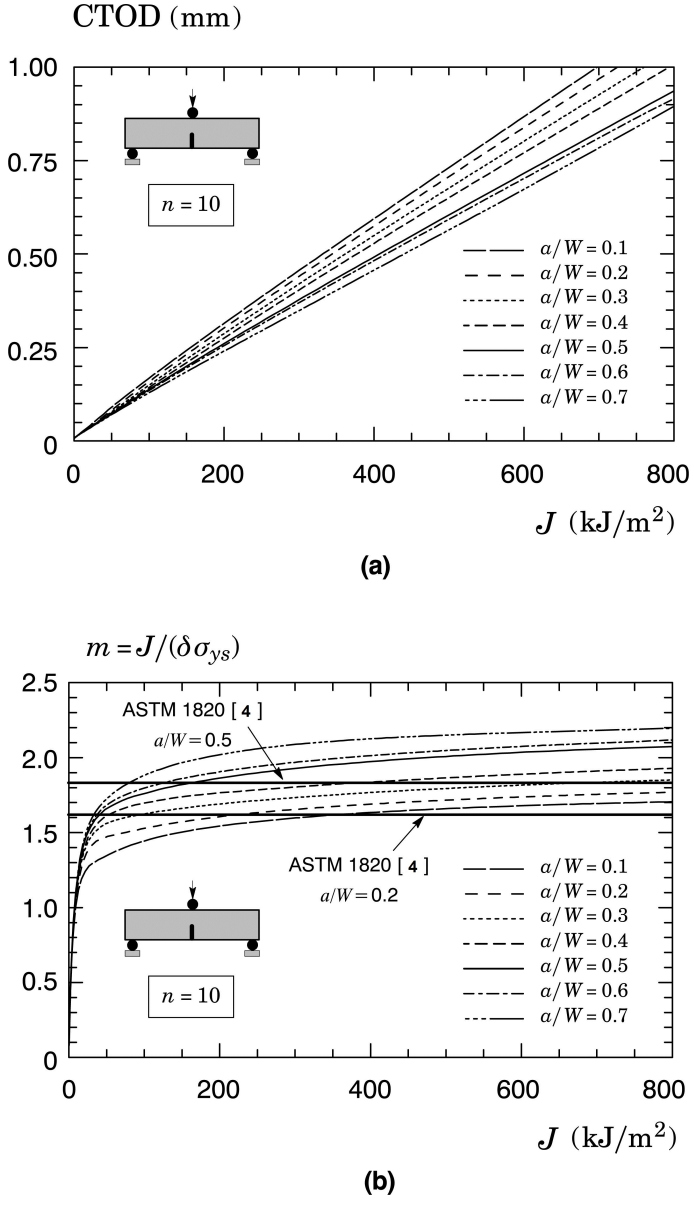

FIGURE 9. J-CTOD relationship for the SE(B) specimen with varying a/W-ratio and $n = 10$ material derived from stationary crack analysis.

Figures 11 and 12 provide the m-values to determine the CTOD for the SE(B) and clamped SE(T) specimens with varying a/W-ratios and strain hardening exponents derived from the plane-strain analyses previously described and reported in previous work [19]. To provide a simpler manipulation of the results displayed in Figs. 11 and 12, a functional dependence of parameter m with crack size, a/W, and hardening exponent, n, is obtained in the form:

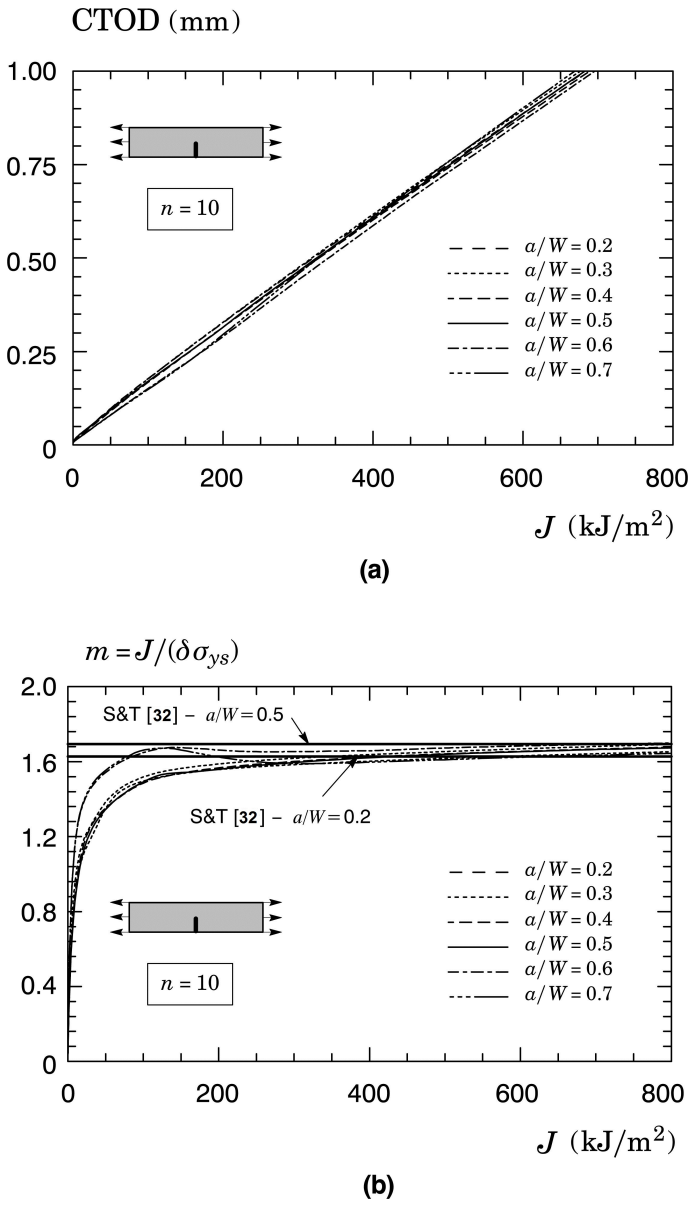

FIGURE 10. J-CTOD relationship for the clamped SE(T) specimen with varying a/W-ratio and $n = 10$ material derived from stationary crack analysis.

$$m = h_1(a/W) + h_2(n) \tag{11}$$

where

$$h_1^{SEB} = -0.194 + 1.077(a/W) - 0.238(a/W)^2 \qquad (12)$$

$$h_2^{SEB} = 14.391n^{-1} + 0.036n \qquad (13)$$

and

$$h_1^{SET} = 0.243 - 0.519(a/W) + 0.742(a/W)^2 \qquad (14)$$

$$h_2^{SET} = 11.545n^{-1} + 0.029n \qquad (15)$$

where it is understood that a multivariate polynomial fitting is adopted to describe the coupled dependence of factor m on the a/W-ratio and hardening exponent n. The above expressions are valid in the range $0.2 \leq a/W \leq 0.7$ and $5 \leq n \leq 20$.

To facilitate comparisons with previous reported results for J-CTOD relationships in SE(B) and clamped SE(T) specimens, Figs. 9-10 also include the m-values derived from previous Eq. (11) for each crack configuration with $a/W = 0.2$ and 0.5 using the strain hardening exponent of $n = 10$ for material employed in the numerical analyses. For the SE(B) specimen, Fig. 9 shows the m-values based on ASTM E1820 [4] whereas Fig. 10 displays m-values derived from 3-D analyses of clamped SE(T) specimens performed by Shen and Tyson (S&T) [32].

Altought an excellent agreement can be seen between the current m results and the reported m-values obtained by S&T' equation [32] and small differences, $\sim$ 12%, using the ASTM E1820 expression [4], a comparison of the m-values has to be done with special care because the m values have been normalized with respect to different reference stresses . The current m-values were based upon the use of σ_{ys} and [4] and [32] used σ_{flow} which is the average value between the 0.2% offset yield strength (σ_{ys}) and the ultimate tensile strength (σ_{TS}). σ_{flow} is typically used to include the influence of plastic yielding upon fracture test parameters.

Being δ inversely proportional to $m \cdot \sigma$, the plastic constraint factor (m) obtained via S&T [32] equation will produce δ estimations lower than current predictions made by Eq. (11). Even though the ASTM E1820 equation [4] produces m values lower than the current proposal, Eq. (11), the final δ value will depend on the material strain hardening. If $\sigma_{flow}/\sigma_{ys} > 1.12$, ASTM E1820-CTOD willl be lower than the CTOD (δ) obtained by Eq. (11).

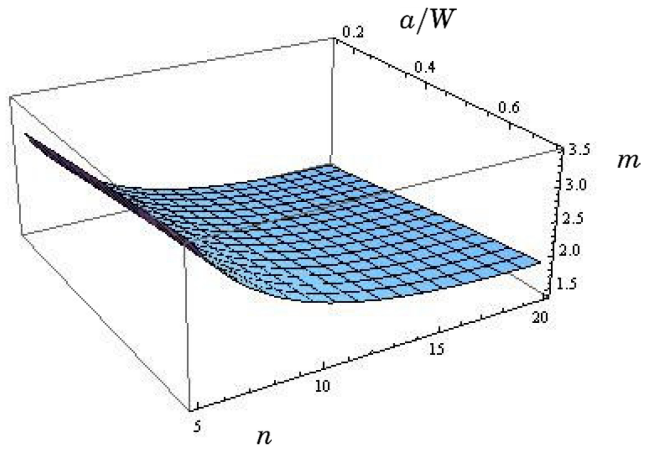

FIGURE 11. Variation of parameter m with a/W-ratio and strain hardening exponent, n, for the analyzed SE(B) specimens.

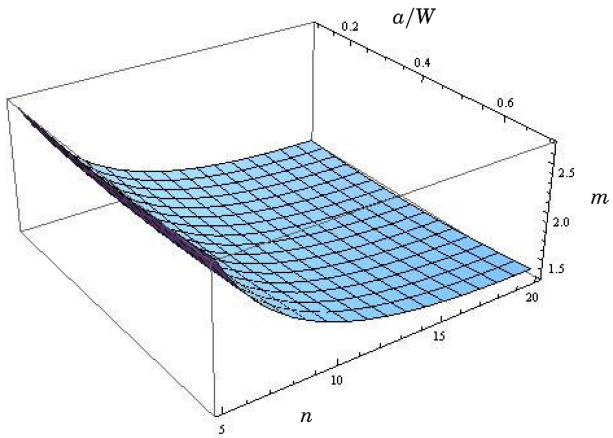

FIGURE 12. Variation of parameter m with a/W-ratio and strain hardening exponent, n, for the analyzed SE(T) specimens.

J-CTOD Relationship in Growing Cracks

We now direct attention to the evolution of CTOD with J with increased amounts of ductile tearing, Δa, for the analyzed crack configurations. The extensive finite element analyses of SE(B) and SE(T) fracture specimens, that include the effects of crack growth, provide a basis to compare the J-CTOD relationship in growing cracks with the variation of J with CTOD for stationary cracks. Here, we adopt the API 5L X70 pipeline grade steel tested by Hippert [27] and described previously to compute crack growth resistance curves for these specimens which in turn serve to determine the CTOD for the advancing crack.

Two different definitions for measuring δ were used during numerical modelling of ductile crack growth as ilustrated in Fig. 2. Using the 90° concept , δ is measured at the current crack tip and the original crack tip. Here, the main goal is to compare which definition of δ correlates better with increasing levels of J.

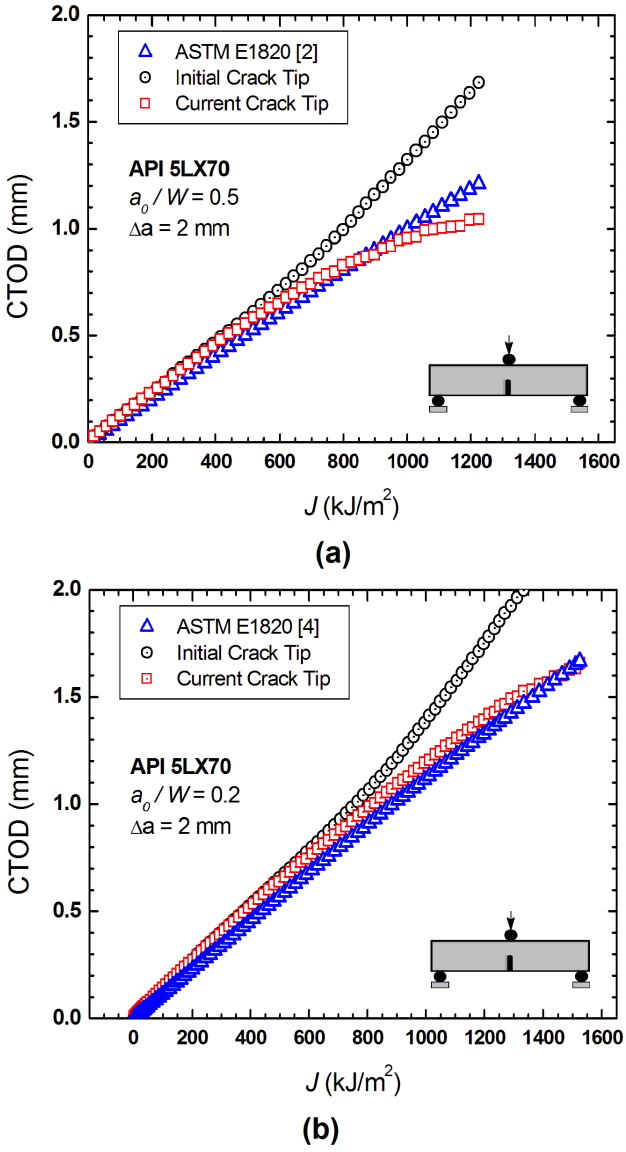

FIGURE 13. Variation of δ with J considering two positions for measuring δ during ductile crack growth: (a) SE(B) geometry with a/W = 0.5; (b) SE(B) geometry with a/W = 0.2 .

First, we focus on the SE(B) geometry with $a/W = 0.2$ and 0.5. Figure 13 shows the evolution of J-CTOD following stable crack growth with increased values of the J-integral. To facilitate comparisons with previous reported results for J-CTOD relationships in SE(B), Fig. 13 shows the CTOD-values based on ASTM 1820 [4]. During the numerical simulation the crack was allowed to grow up to $\Delta a = 2$ mm.

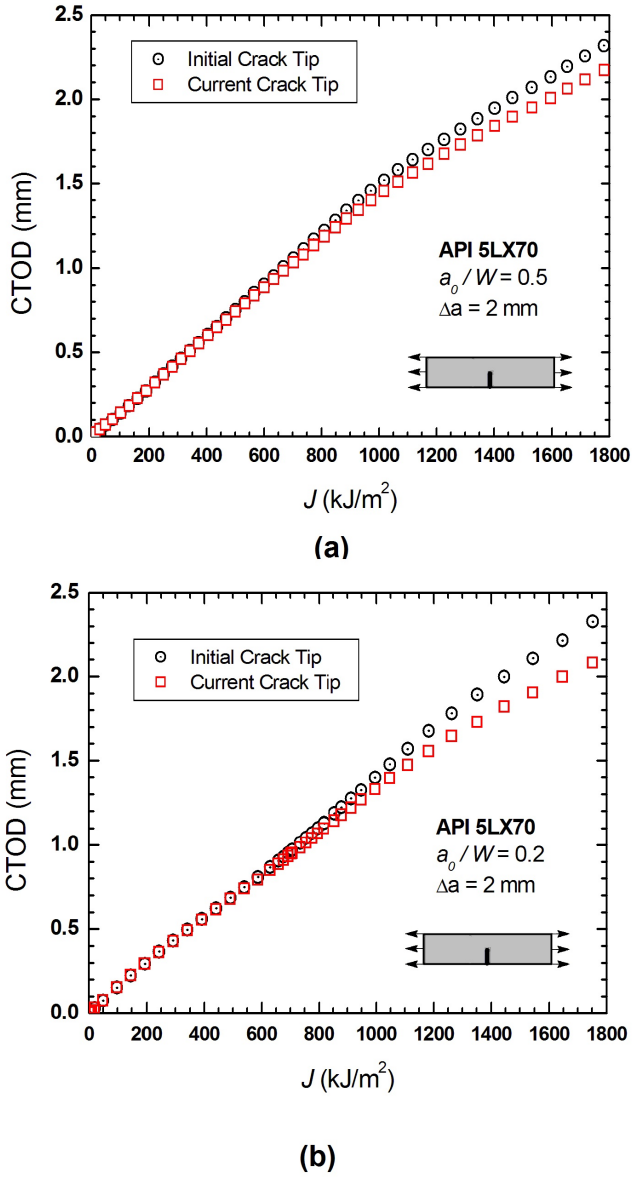

FIGURE 14. Variation of δ with J considering two positions for measuring δ during ductile crack growth: (a) SE(T) geometry with a/W = 0.5; (b) SE(T) geometry with a/W = 0.2.

Clearly, there is a good linear relationship between J and

CTOD when δ is measured in its initial position. On the other hand, when the CTOD is measured in the current crack position there is a departure from linearity between J and CTOD for both crack size ratios. However, the prediction of δ made by ASTM 1820 [4] is close to δ measured at the current crack tip.

Next, we focus on studying the influence of the position where δ is measured for SE(T) specimens. Figure 14 shows the evolution of J-CTOD following stable crack growth for two crack size ratios. For this geometry, δ is almost independent of where it is measured. However, small differences for $\Delta a > 1.5$ mm and shallow cracks can be seen in Figure 14.b

Figures 15-16 provide the variation of the J-integral with CTOD under increasing level of deformation for the SE(B) and clamped SE(T) fracture specimens with different a/W-ratios, derived from the crack growth analyses up to $\Delta a = 2$ mm. To facilitate comparisons with the stationary crack results, these plots include the m-values dependency with crack size derived from previous Eq. (11), ASTM E1820 [4] and S&T [32] equations for each crack configuration with initial crack size ratios $a_0/W = 0.2, 0.3, 0.4$ and 0.5 , using the strain hardening exponent of $n = 13.3$ for the API X70 material employed in the numerical analyses. For each pre-cracked specimen, instantaneous values of m [$m_i = f(\mathrm{J}_i, \delta_i)$] are reported for $\Delta a = 0.5, 1, 1.5$ and 2.0 mm in Figs. 15-16.

First, the SE(B) results are analyzed. The crack growth results bring out only small deviations from linearity between J and CTOD. The instantaneus values of m during ductile crack growth decreased on average about 12% for all SE(B) plain-strain models. For the API X70 material, estimated m-values, made by Eq. (11) and ASTM E1820-Equation [4], were almost identical as can be seen in Fig. 15.(b) . However, ASTM-δ predictions will be lower than the predictions made by Eq. (11) because the ASTM-δ is based on σ_{flow} rather than σ_{ys} as previously discussed.

In particular, there is almost no difference between the m-values derived from a stationary crack analysis and m predictions for specimens which have experienced small crack growth $\Delta a \leq 0.5$. However, large amounts of crack propagation $\Delta a \leq 1.5$ produce differences in measured and predicted m-values around 20% for all pre-cracked SE(B) specimen having different initial crack size ratios. Considering this reduction on m-values during ductile crack growth as a good representation of real behavior for SE(B) specimens, CTOD estimations based on stationary cracks analyses will be underpredicted if either [4] or Eq. (11) is used.

Finally, the SE(T) results are commented. The crack growth results clearly reveal a rather weak effect of ductile tearing on the J-CTOD linear relationships and, consequently, on the evolution of parameter m with increased J for the analyzed SE(T) fracture specimens. Fig. 16.(b) shows increased m-values during ductile crack growth analyses for SE(T) geometries under plane strain conditions. m-values predicted by Eq. (11) show very small variations with crack size as observed in Fig. 10.(b).

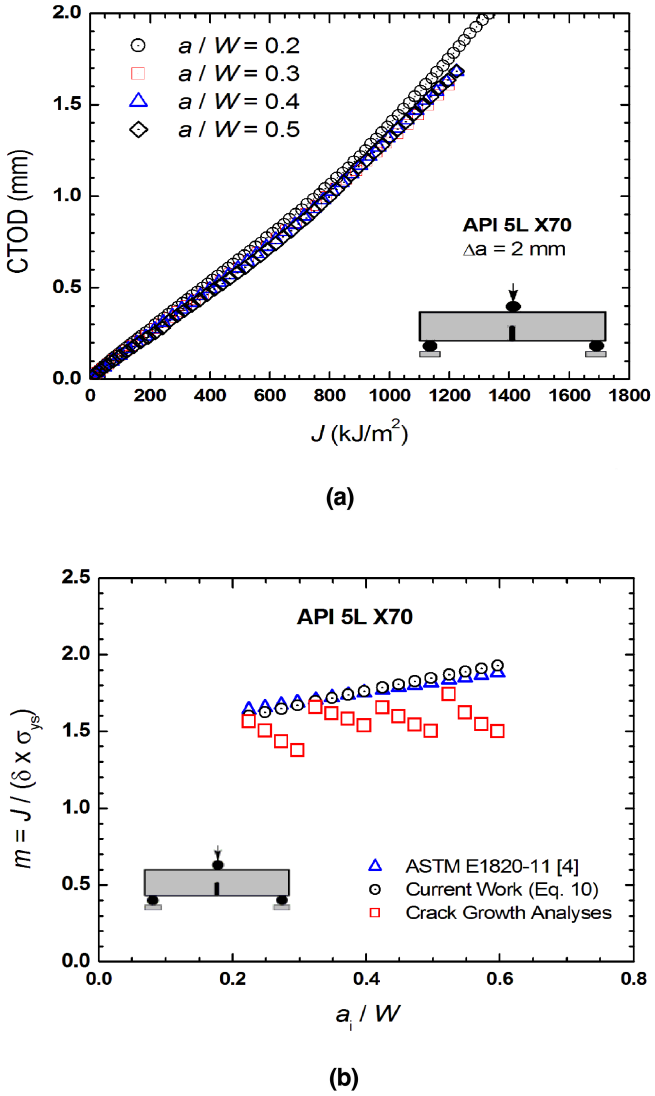

FIGURE 15. (a) J-CTOD relationship for the SE(B) specimen with varying a/W-ratio and API X70 material derived from the crack growth analysis;(b) Evolution of m-values with crack size.

In particular, the m-values derived from a stationary crack analyses for the clamped SE(T) specimens using Eq. (11) are in very close agreement with the corresponding values derived from the growth analyses. On the other hand, m-values obtained by S&T [32] equation are lower than predicted by crack growth analyses, specially for shallow cracks with differences around 60%, and deep cracks have differences around 20%. Therefore, S&T' equation [32] will produce higher estimations of δ, when compared to the current proposal, Eq. 11, unless $(\sigma_{flow}/\sigma_{ys}) > (\mathrm{m}_{Eq.(11)}/\mathrm{m}_{ASTME1820})$

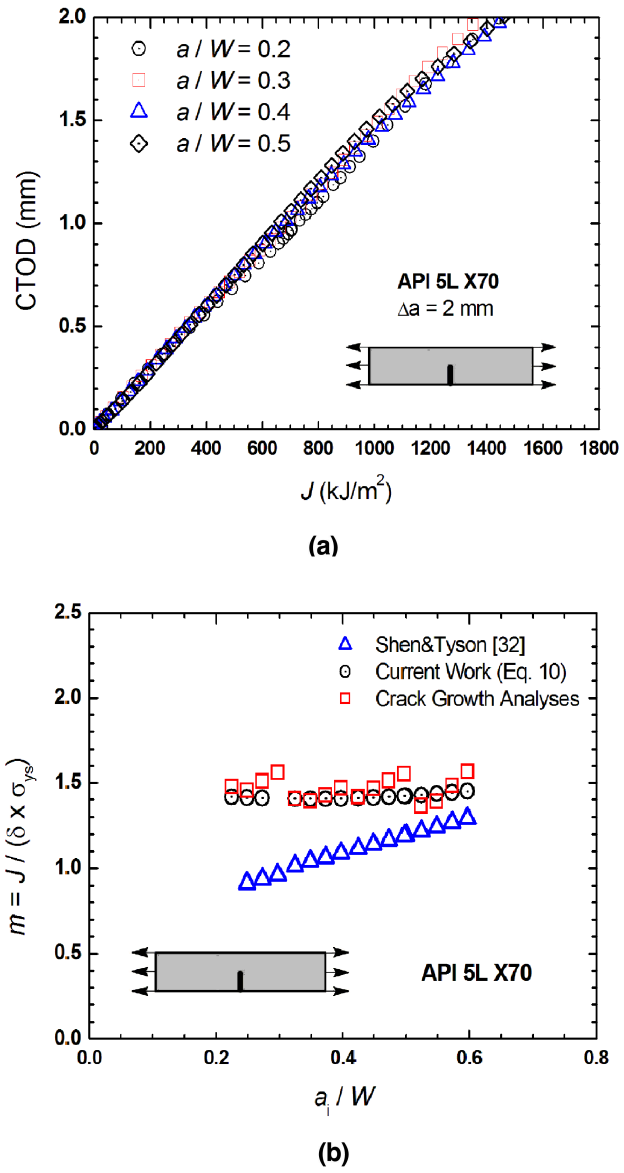

FIGURE 16. (a) J-CTOD relationship for the clamped SE(T) specimen with varying a/W-ratio and API X70 material derived from the crack growth analysis;(b) Evolution of m-values with crack size.

CONCLUDING REMARKS

The extensive set of nonlinear finite element analyses for detailed plane-strain models of SE(B) and clamped SE(T) fracture specimens with varying crack sizes and straing hardening properties described here provide the basis to determine accurate relationships between J and CTOD for use in testing protocols for toughness measurements.

These analyses include stationary and crack growth plane-strain results to determine J and CTOD for SE(B) and clamped SE(T) cracked configurations based on load-displacement records. Non-linear 2D finite element studies have shown that J-CTOD relationship is independent of initial crack size ratio for SE(T) specimens under stationary and growing analyses .Also, the results described here clearly reveal a rather weak effect of ductile tearing on the J-CTOD relationships for SE(T) specimens with different initial crack size ratios ($0.2 \leq a/W \leq 0.5$) and, consequently, on the evolution of parameter m with increased J values. ASTM E1820 predictions of δ, based on J values, will be lower than predictions made by current proposal. Current procedures to determine CTOD-values from first evaluating the plastic component of J using the plastic work defined by the area under the load vs. CMOD curve and then converting it into the corresponding value of plastic CTOD provide accurate measurements of crack growth response in terms of CTOD $-$ R curves.

ACKNOWLEDGMENT

This investigation is supported by Fundação de Amparo à Pesquisa do Estado de São Paulo Paulo (FAPESP) through research grant 2012/00094-2 and 2013/01139-2 provided to the first author (DFBS). The work of CR is supported by the Brazilian Council for Scientific and Technological Development (CNPq) through Grants 304132/2009-8 and 476581/2009-5. The authors are indebted to Dr. Eduardo Hippert Jr. (PETROBRAS) for providing the motivation to this work and for the many helpful and insightful discussions on testing protocols for crack growth measurements.

REFERENCES

[1] Martin, J., and Koers, R., 1998. Ctod versus j-integral as a fracture parameter.

[2] Anderson, T. L., 1988. "A comparison of J-Integral and ctod as fracture toughness parameters". *ASTM STP 945*, pp. 741–753.

[3] Wilson, C., and Landes, J., 1994. "Inconsistencies between CTOD and J calculations". *Journal of Testing and Evaluation,* ***22***, pp. 505–511.

[4] American Society for Testing and Materials, 2011. Standard test method for measurement of fracture toughness, ASTM E1820-2011.

[5] ASTM, 2008. "Standard test method for measurement of fracture toughness.". *American Society for Testing and Materials, ASTM E1290*.

[6] Shih, C., 1981. "Relationships between the J-Integral and the crack opening displacements for stationary and extending cracks". *Journal of the Mechanics and Physics of Solids,* ***29***, pp. 305–326.

[7] DNV, 2007. Submarine pipeline systems. Tech. rep., Det Norsk Veritas, DNV-OS-F101.

[8] Det Norske Veritas, 2006. Fracture control for pipeline installation methods introducing cyclic plastic strain, DNV-RP-F108.

[9] Cravero, S., and Ruggieri, C., 2007. "Further developments in J evaluation procedure for growing cracks based on LLD and CMOD data". *International Journal of Fracture,* ***148***, pp. 347–400.

[10] Shen, G., and Tyson, W. R., 2009. "Crack size evaluation using unloading compliance in single-specimen single-edge notched tension fracture toughness testing". *Journal of Testing and Evaluation,* ***37***(4), p. JTE102368.

[11] Nyhus, B., 2001. State of the art for the use of SE(T) specimens to test fracture properties in pipes for reeling. Tech. rep., SINTEF Materials Technology.

[12] Park, D. Y., Tyson, W. R., Gianetto, J. A., Shen, G., and Eagleson, R. S., 2010. "Evaluation of fracture toughness of X100 pipe steel using SE(B) and clamped SE(T) single specimens". *International Pipeline Conference (IPC).*

[13] Ruggieri, C., 2012. "Further results in J and CTOD evaluation procedures for SE(T) fracture specimens- part I: Homogeneous materials". *Engineering Fracture Mechanics,* ***79***, pp. 245–265.

[14] Paredes, M., and Ruggieri, C., 2012. "Further results in J and CTOD estimation procedures for SE(T) fracture specimens - Part II: weld centerline cracks". *Engineering Fracture Mechanics,* ***89***, pp. 24–39.

[15] Anderson, T. L., 2005. *Fracture Mechanics: Fundaments and Applications - 3rd Edition*. CRC Press, Boca Raton, FL.

[16] Tada, H., Paris, P. C., and Irwin, G. R., 2000. *The Stress Analysis of Cracks Handbook*, 3rd ed. American Society of Mechanical Engineers.

[17] Cravero, S., and Ruggieri, C., 2005. "Correlation of fracture behavior in high pressure pipelines with axial flaws using constraint designed test specimens - Part I: Plane-strain analyses". *Engineering Fracture Mechanics,* ***72***, pp. 1344–1360.

[18] Kirk, M. T., and Dodds, R. H., 1993. "J and CTOD estimation equations for shallow cracks in single edge notch bend specimens". *Journal of Testing and Evaluation,* ***21***, pp. 228–238.

[19] Sarzosa, D. F. B., and Ruggieri, C., 2014. "Relationship between J and ctod in se(t) and se(b) specimens for stationary and growing cracks". In International Pipeline Conference (IPC).

[20] Xia, L., and Shih, C. F., 1995. "Ductile crack growth - I: A numerical study using computational cells with microstructurally-based length scales". *Journal of the Mechanics and Physics of Solids,* ***43***, pp. 223–259.

[21] Gurson, A., 1977. "Continuum theory od ductile rupture by void nucleation and growth: Part I-Yield criteria and flow rules for porous dutile media". *Journal of Engineering Materials and Technology,* ***99***, pp. 2–15.

[22] Tvergaard, V., 1990. "Material failure by void growth to coalescence". *Advance in Applied Mechanics,* ***27***, pp. 83–151.

[23] Xia, L., and Shih, C., 1995. "Ductile crack growth-II. void nucleation and geometry effects on macroscopic fracture behavior". *Journal of the Mechanics and Physics of Solids,* ***43***, pp. 1953–1981.

[24] Ruggieri, C., and Dodds, R., 1996. "Numerical modeling of ductile crack growth using computational cell elements". *International Journal of Fracture,* ***82***, pp. 67–95.

[25] Gullerud, A., Gao, X., Dodds, R., and Haj-Ali, R., 2000. "Simulation of ductile crack growth using computational cells: Numerical aspects". *Engineering Fracture Mechanics,* ***66***, pp. 65–92.

[26] Ruggieri, C., and Dotta, F., 2011. "Numerical modeling of ductile crack extension in high pressure pipelines with longitudinal flaws". *Enginering Structures,* ***33***, pp. 1423–1438.

[27] Hippert, E., 2001. "Experimental investigation of ductile fracture behavior in API X70 grade pipeline steels and applicability of crack growth resistance curves to predict the burst pressure in longitudinally cracked pipes". PhD thesis, Polytechnic School, University of São Paulo. (In Portuguese).

[28] American Petroleum Institute, 2007. Fitness-for-service, API RP-579-1 / ASME FFS-1.

[29] Faleskog, J., and Shih, C., 1998. "Cell model for nonlinear fracture analysis - I: Micromechanics calibration". *International Journal of Fracture,* ***89***, pp. 355–373.

[30] Gullerud, A., Koppenhoefer, K., Roy, A., RoyChowdhury, S., Walters, M., and Dodds, R. J., 2008. "Warp3D-release 15.9: 3-D dynamic nonlinear fracture analysis of solids using parallel computers and workstations".

[31] Hippert, E., and Ruggieri, C., 2001. "Experimental and numerical investigation of ductile crack extension in a high strength pipeline steel". In ASME 2001 Pressure Vessels & Piping Conference (PVP 2001) .

[32] Shen, G., and Tyson, W. R., 2009. "Evaluation of ctod from j-integral for se(t) specimens". In Pipeline Technology Conference (PTC 2009) .